

Master's Thesis

Coil-Array Inductive Power Transfer System for Autonomous Underwater Vehicle

Yu Cheng

Program of Information Science and Engineering
Graduate School of Information Science
Nara Institute of Science and Technology

Supervisor: Professor Minoru Okada
Network Systems Lab. (Division of Information Science)

January 23, 2021

A Master's Thesis
submitted to Graduate School of Information Science,
Nara Institute of Science and Technology
in partial fulfillment of the requirements for the degree of
MASTER of ENGINEERING

Yu Cheng

Thesis Committee:

Professor Minoru Okada
(Supervisor, Division of Information Science)
Professor Yuichi Hayashi
(Co-supervisor, Division of Information Science)
Associate Professor Takeshi Higashino
(Co-supervisor, Division of Information Science)
Assistant Professor Quang-Thang Duong
(Co-supervisor, Division of Information Science)
Assistant Professor Na Chen
(Co-supervisor, Division of Information Science)

Coil-Array Inductive Power Transfer System for Autonomous Underwater Vehicle*

Yu Cheng

Abstract

For a long time, providing a stable, safe, and efficient power supply for underwater electromechanical equipment has always been a concern in deep-sea exploration. Compared with the complicated docking mechanism, potential safety hazards, and expensive price of traditional wet-mate connectors, wireless power transmission (WPT) technology can transmit energy without any electrical contact between the power supply and the electrical equipment, which provides an effective solution to the aforementioned drawbacks of wired charging. There are many uncontrollable factors in the seawater working environment. Therefore, this topic takes the equivalent circuit and magnetic field distribution as the theoretical basis to study the energy transmission characteristics of underwater WPT and proposes corresponding improvements and solutions to the current problems and deficiencies. Especially for the unstable output voltage of the receiver and excessive magnetic flux density at the internal of AUV. This paper proposes a new type of UWPT system with a coil-array structure, which can reduce the magnetic flux density at the center of the AUV by 40% compared to the conventional cylindrical structure.

Keywords:

Autonomous underwater vehicle, inductive power transfer, underwater wireless power transfer, undersea

*Master's Thesis, Graduate School of Science and Technology, Nara Institute of Science and Technology, January 23, 2021.

Contents

List of Figures	iv
List of Tables	vi
1 Introduction	1
1.1 Background and research purpose	1
1.2 Wireless power transfer technologies	3
1.3 Underwater wireless power transfer	4
1.3.1 Underwater environment	5
1.3.2 Common UWPT systems	6
1.4 The main research content of this thesis	7
1.5 Roadmap	7
2 Basic principles of IPT	9
2.1 Inductive coupling model	9
2.2 Compensation network technologies	10
2.2.1 S-S compensation topology	11
2.2.2 CLC-S compensation topology	12
2.3 Underwater WPT system model	13
3 Preliminary exploration of underwater IPT system	15
3.1 The system in three different media	15
3.2 The system in different sizes of the coil	17
3.3 The system in different frequency	19
3.4 Conclusion	19
4 Coil-array WPT	22
4.1 Measurement of the coil-array WPT system	23

4.2	The other coil arrangements and comparison	26
4.3	Magnetic field distribution	27
4.3.1	Magnetic field distribution of two-ring strcture	29
4.3.2	Magnetic field distribution of coil-array strcture	31
4.4	PET over shift in two directions	31
5	Conclusion	34
5.1	Future works	34
References		36

List of Figures

1.1	Underwater sensor networks architecture [9].	2
1.2	Near-field wireless power transfer.	4
1.3	Far-field wireless power transfer.	5
1.4	Stacked UWPT system [18].	6
1.5	The primary and secondary coils of stacked UWPT system [18].	6
1.6	Plug-in UWPT system [19].	7
2.1	Inductive coupling model.	9
2.2	Equivalent circuit of inductive coupling model.	10
2.3	Compensation networks.	11
2.4	S-S structure.	12
2.5	CLC-S structure.	13
2.6	Equivalent circuit of the coil under seawater.	14
3.1	Two-ring structure.	15
3.2	Two-ring structure ($r_{inner} = 50mm$, $r_{outer} = 80mm$).	17
4.1	Coil-array structure.	22
4.2	Sechematic diagram of coil-array UWPT system.	23
4.3	Coil-array IPT structure (Both sides with ferrite tile), inner coil in the center or the outer coil.	24
4.4	Measurement of L_s	24
4.5	Equivalent circuit of two coil model.	25
4.6	Coil-array IPT structure (both sides without ferrite tile), inner coil in the center of the outer coil (left), inner coil next to the outer coil (right).	26

4.7	Coil-array IPT structure (both sides without ferrite tile), inner coil in the center of the outer coil (left), inner coil next to the outer coil (right).	27
4.8	Coil-array IPT structure (inner small coils with ferrite tile, outer small coils without ferrite tile), inner coil in the center of the outer coil (left), inner coil next to the outer coil (right).	28
4.9	Two kind of UWPT coil structure simulation diagram.	29
4.10	Magnetic field distribution of two-ring IPT structure.	29
4.11	Cross-sectional view of the magnetic field distribution of two-ring IPT structure.	30
4.12	Magnetic field distribution of coil-array IPT structure.	30
4.13	Cross-sectional view of the magnetic field distribution of aoil-array IPT structure.	31
4.14	Equivalent circuit of two coil model.	32
4.15	The PET over shift in two different directions.	33
4.16	The PET over different resistance of load (coil-array structure). .	33

List of Tables

1.1	The different wireless power transmission technologies.	3
2.1	The dielectric constant & conductivity of some materials at 25°C under 1kHz [21, 22].	13
3.1	The parameters of ring coil structure.	16
3.2	The parameters of ring coil structure.	17
3.3	Z-parameters in different distance and media	18
3.4	The parameters of ring coil structure.	19
3.5	Z-parameters in different frequencies and media	20
4.1	The parameters of coil-array structure.	23
4.2	Maximum power transfer efficiency of different coil arrangements.	27
4.3	The parameters of two coil structure in simulation.	28

1 Introduction

1.1 Background and research purpose

In the foreseeable future, the electrification of ocean systems, renewable ocean power sources, and ocean energy networks will be necessary, which will help accelerate the growth and deployment of ocean renewable energy and ways to explore and understand the ocean [1, 2]. To achieve electrification in the ocean, it is necessary to deploy corresponding sensor networks underwater and process the data received by underwater sensors in a timely manner (Figure 1.1). At the same time, underwater sensors are also an essential tool for studying the marine environment [3, 4]. They can easily and flexibly explore underwater terrain and ecological environment, which provides convenience for the deployment of underwater sensor networks. An excellent AUV needs to have good equipment waterproofness, long-distance underwater controllability, and power durability. For the water-resistance of the equipment, we can use high-performance waterproof and pressure-resistant materials [5–7]. The remote controllability needs to solve the problems of long-distance underwater wireless communication. The durability of electrical equipment requires low energy consumption AUV and high-energy batteries or a continuous power supply. Sufficient power supply can keep underwater sensors and AUVs in an efficient and stable working state for a long time [8]. Indirectly, reducing human interference when electrical equipment is working underwater can also improve work efficiency and reduce deployment costs. Therefore, the power supply for underwater electrical equipments has become a novel research direction. Such methods can solve the energy supply problem of underwater equipment economically and ensure the system to perform long-term and stable work.

In traditional marine engineering, power is supplied to underwater equipment

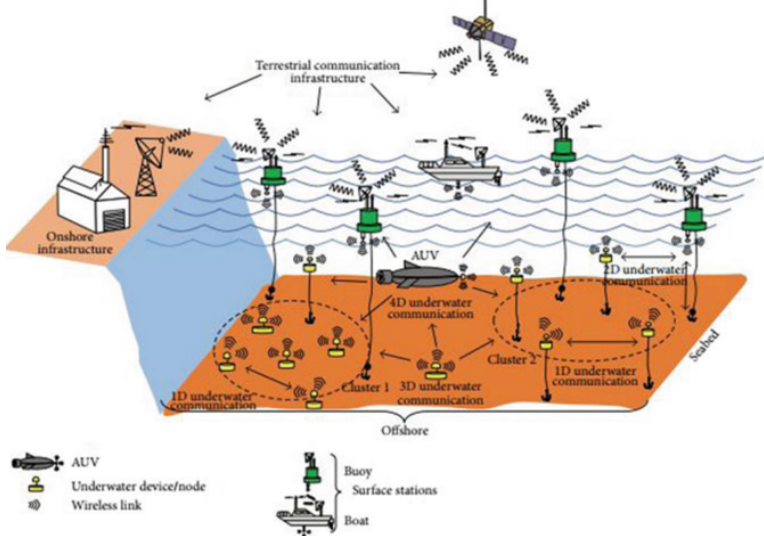


Figure 1.1: Underwater sensor networks architecture [9].

through wet-mate subsea connectors [10]. For the traditional wet plug interface technology, its high cost, complex docking method, poor safety performance, and easy to be corroded by seawater, make its disadvantages in marine engineering increasingly obvious. Wireless power transfer (WPT) simplifies the connection between underwater equipment and power supply, reduces the continuous operating cost of underwater equipment, saves a lot of resources, and gradually gains the favor of scholars.

The ocean itself and its surroundings contain a lot of energy, such as tidal energy, wave energy, marine current power, ocean thermal energy, and sea salinity gradient power [11–14]. Ocean energy is rich, widely distributed, clean, and pollution-free, but low energy density and strong regionality. These advantages make it attractive as grid-connected energy, and may also make it an isolated and remote ocean energy source, thereby providing a valuable source of ocean space. Continuous development provides power solutions that are attractive. The rapid development of distributed ocean energy applications (such as underwater sensor networks, ocean sensors and monitoring technologies, ocean automatic network buoys, and deep-sea and tsunami buoys) is beneficial. In particular, it can power an autonomous underwater vehicle (AUV) whose service life is limited by its battery power.

Table 1.1: The different wireless power transmission technologies.

Technology	Range	Frequency	Antenna devices	Applications
Microwaves	hm – km	GHz	Parabolic dishes, phased arrays, rectennas	Satellite, drone aircraft
Optical	dam – km	\geq THz	Lasers, photocells, lenses	Drone aircraft, space elevator
Capacitive	cm – m	kHz – MHz	Metal plate electrodes	Smartcards, biomedical implant
Inductive	mm – m	Hz – GHz	Tuned wire coils, lumped element resonators	Electric toothbrush, smartphone, electric vehicle

1.2 Wireless power transfer technologies

Broadly speaking, power transfer without direct electrical contact between the primary and secondary is wireless power transfer. Wireless power technology can be divided into two main categories, near-field (nonradiative region) power transfer and far-field (radiative region) power transfer. Near-field means the area within about 1 wavelength (λ) of the antenna. The range of near-field devices is conventionally divided into two categories [15] (Suppose the distance between two antennas is represented by D_{range} , and the diameter of two antenna coils is represented by $D_{ant.}$):

- Short range, the distance between two antennas is less than the diameter of antenna: $D_{range} \leq D_{ant.}$. In this range, power is usually transferred through non-resonant capacitive or inductive coupling.
- Mid-range, the distance between two antennas is less than 10 times the diameter of antenna: $D_{range} \leq 10D_{ant.}$. In this range, energy is usually transferred through resonant capacitive or inductive coupling.

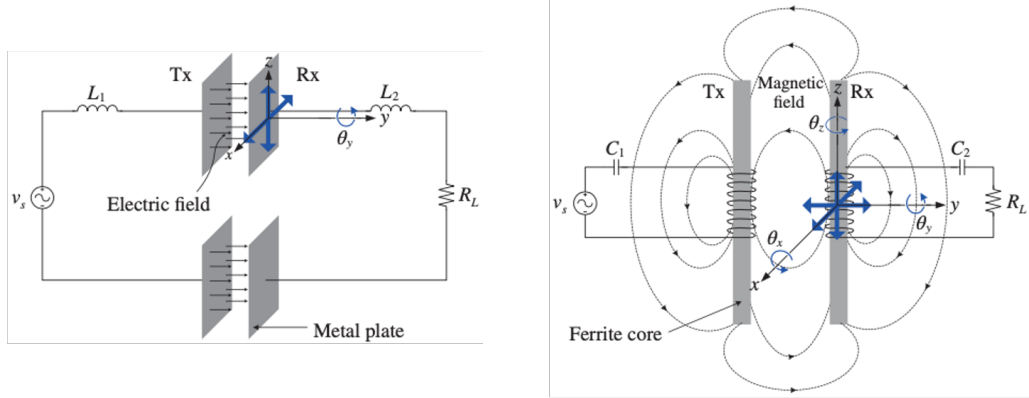
Far-field or radiative region, power is transmitted by means of electromagnetic waves, like radio waves, microwaves, or light waves. When the operating frequency (f) is relatively low, wavelength $\lambda = c/f$, at this time the diameter of the

antenna is much smaller than the wavelength, $D_{ant} \ll \lambda$, and the radiated power will be very small. When the diameter of antenna is about wavelength, $D_{ant} \approx \lambda$, radiate power will be efficient. When the diameter of antenna is much great than wavelength, $D_{ant} \gg \lambda$, we can using high-gain antennas to concentrate electromagnetic waves on a narrow beam and directly aim at the receiver to improve transmission efficiency.

Therefore, near-field wireless power transfer systems mainly include inductive coupling power transfer and capacitive coupling power transfer (Figure 1.2). Far-field wireless power transfer systems mainly include microwave, optical, and acoustic power transfer (Figure 1.3). The respective characteristics are shown in the table 1.1.

1.3 Underwater wireless power transfer

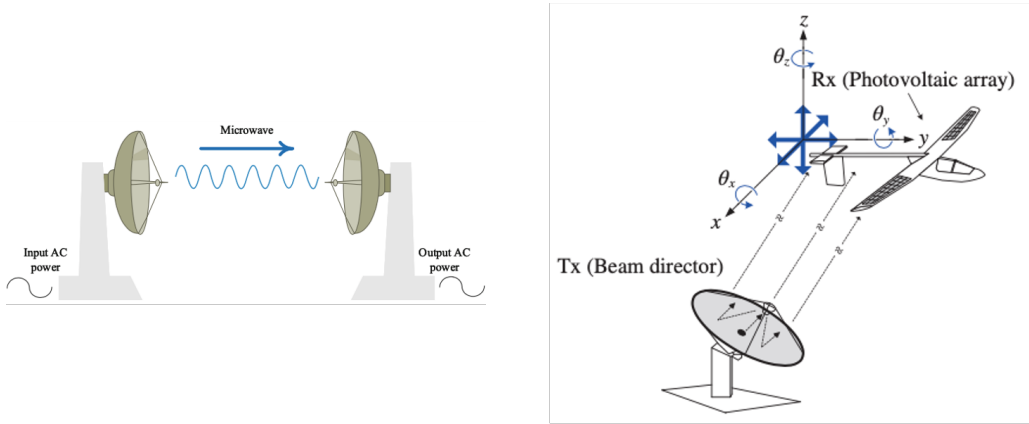
WPT technology has unique advantages in special environments, and along with the continuous development of landing application research and the emergence of a large number of results [17], it has attracted the attention of underwater technology researchers.



(a) Capacitive power transfer [16].

(b) Inductive power transfer [16].

Figure 1.2: Near-field wireless power transfer.



(a) Microwave power transfer [1].

(b) Laser power transfer [16].

Figure 1.3: Far-field wireless power transfer.

1.3.1 Underwater environment

In the seawater environment, we usually need to consider the following points.

- Underwater, seawater has a blocking effect on high-frequency electromagnetic waves. The distance of electromagnetic waves propagating underwater is inversely proportional to the frequency, making it difficult to achieve long-distance power transmission.
- Conductivity, due to the electrical conductivity of seawater, traditional wireless power transmission analysis methods are no longer applicable. At present, the system modeling and related theoretical analysis of underwater wireless power transfer technology need to be improved.
- Undercurrent, the submarine landform is complex and there is undercurrent. The coupler core is liable to drift under water, and there are problems such as difficulty in docking, which results in low transmission efficiency.
- Some other imprints, like microbial enrichment, temperature, salinity, etc.

1.3.2 Common UWPT systems

Figure 1.4 shows a stacked UWPT system, this study was completed by Baowei Song et al [18]. They achieved a transmission efficiency of 72% while maintaining 100w output power. They are using a saddle structure transmitter (Details as shown in figure 1.5) and a deformed cylindrical receiver. This structure is very convenient for AUV to park, but because there is no stable protection structure, it is also easy to shift when charging.

Figure 1.6 shows the plug-in UPWT system. We can observe that the AUV needs to be moved into a hollow cylindrical structure transmitter, which makes it difficult to park. However, this structure can maintain the stability of the AUV during AUV charging, so that the system charging is more secure. Another advantage of this structure is that the receiving coil is relatively large, which can make the mutual inductance high. And we can use this system to transmit larger power. Therefore, our coil-array structure UWPT system is built on this structure.

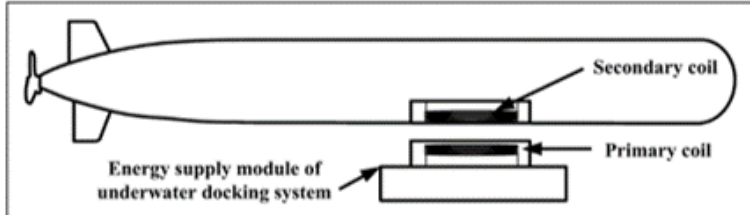


Figure 1.4: Stacked UWPT system [18].

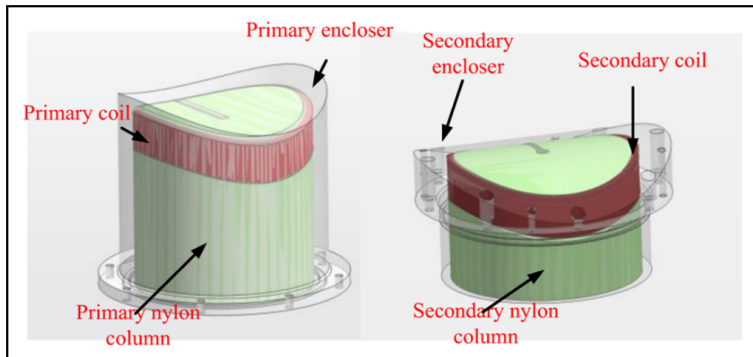


Figure 1.5: The primary and secondary coils of stacked UWPT system [18].

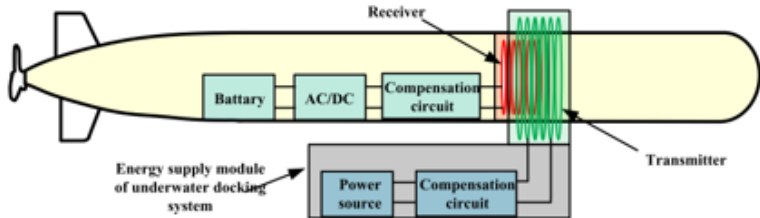


Figure 1.6: Plug-in UWPT system [19].

1.4 The main research content of this thesis

This thesis mainly studies the underwater wireless power transfer system, and analyzes the difference between the underwater environment and the land environment WPT system. Considering the durability and high reliability of underwater AUV, we propose a novel coil-array power transfer system. It provides reference materials for the subsequent research on the wpt system of multiple coil groups.

1.5 Roadmap

The first chapter analyzes the background of this research and its research purpose and significance, analyzes the characteristics and advantages and disadvantages of mainstream WPT technology, and provides a basis for using IPT technology as an underwater wireless energy transmission system in the following text. A detailed summary and analysis of the current research status of related technologies at home and abroad, including underwater wired energy transmission technology, WPT technology in underwater and air media, and an explanation of the research focus of this article.

The second chapter focuses on the analysis of the basic theory of wireless energy transmission. First, the basic IPT model is explained, and its working principle is analyzed. Then explained the related technology of compensation network. Finally, analyze the underwater IPT system model.

The third chapter initially explores the influence of the underwater environment on the scene wpt system. First, by measuring the Z-parameter in three different media to observe the changes of the wpt system parameters in different media.

Then by changing the size of the internal coil to change the distance between the coils, to judge the change of the wpt system parameters at different distances. Finally, by changing different working frequencies, we can observe the changes of system parameters under different comments.

The fourth chapter first studies the magnetic field characteristics of the different coil structures, focusing on the analysis of the coil size and distance effect on the coil magnetic field, and simulates the magnetic field distribution of the coil containing the air gap core, and proposes a new type of coil-array structure. The simulation was carried out by Wipl-d software, and the magnetic field distribution and system transmission efficiency of the coil-array coil structure and the two-ring structure were compared. Then through experiments, we compared the performance of several different coil-array arrangements. Summarize the pros and cons of different arrangements.

Chapter five summarizes the experimental results and some shortcomings in the previous article. In response to these shortcomings, some suggestions that can improve the performance of the experiment are put forward, which are written in the future work.

2 Basic principles of IPT

This chapter will first introduce the principle of IPT technology from the physical level, and then introduce the principle of IPT technology from the circuit level, analyze the relationship between different equivalent models, and derive system energy transmission indicators that can represent system performance. And analyze the influence of relevant design parameters on system transmission performance. Analyze the influence of the medium on the system performance in the WPT process, and propose an equivalent model in the underwater working environment. Perform simulation analysis on the derivation to ensure that complete theoretical support is provided for more detailed theoretical research and research on new IPT technology.

2.1 Inductive coupling model

Figure 2.1 depicts the circuit model of IPT systems, where the transmitting coil L_1 and the receiving coil L_2 are directly connected to the power source and the load, respectively. Denote M as the mutual inductance, r_1 and r_2 as the equivalent AC resistance of coils.

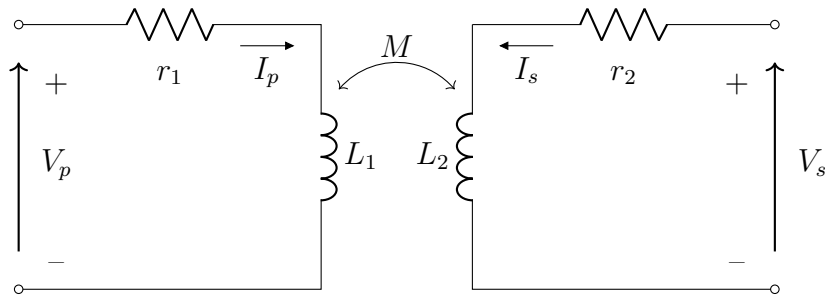


Figure 2.1: Inductive coupling model.

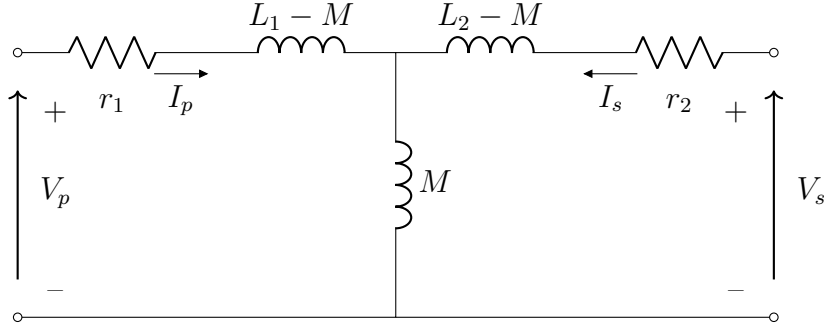


Figure 2.2: Equivalent circuit of inductive coupling model.

Therefore, the equivalent circuit can be expressed as figure 2.2. According to the Kirchhoff's circuit laws. The following formulas can be easily found.

$$V_p = I_p[r_1 + j\omega(L_1 - M)] + (I_p + I_s)j\omega M \quad (2.1)$$

$$= r_1 I_p + j\omega L_1 I_p - j\omega M I_p + j\omega M I_p + j\omega M I_s \quad (2.2)$$

$$= (r_1 + j\omega L_1) I_p + j\omega M I_s \quad (2.3)$$

$$V_s = j\omega M I_p + (r_2 + j\omega L_2) I_s \quad (2.4)$$

The above equations can be expressed as the following matrix equation.

$$\begin{bmatrix} V_p \\ V_s \end{bmatrix} = \begin{bmatrix} r_1 + j\omega L_1 & j\omega M \\ j\omega M & r_2 + j\omega L_2 \end{bmatrix} \begin{bmatrix} I_p \\ I_s \end{bmatrix} \quad (2.5)$$

If we use \mathbf{V} , \mathbf{Z} , \mathbf{I} to express the corresponding matrices. The formula 2.5 can be represented as follows.

$$\mathbf{V} = \mathbf{Z} \cdot \mathbf{I} \quad (2.6)$$

Here, the imaginary part of Z_{11} ($j\omega L_1$) and Z_{22} ($j\omega L_2$) can be canceled by the compensation networks.

2.2 Compensation network technologies

A compensation network is a network that makes some adjustments to compensate for system electrical defects. If capacitor compensation is used only on the

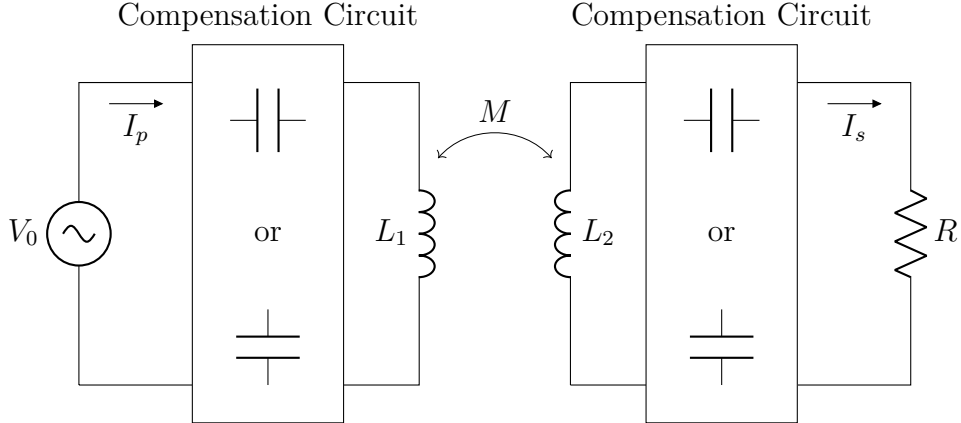


Figure 2.3: Compensation networks.

primary or secondary side, it is called single-sided compensation topology; when capacitor compensation is used on both the primary and secondary sides at the same time, it is called double-sided compensation topology. The calculation of the capacitance value of single-sided compensation is relatively simple, but the actual effect is not as good as the double-sided compensation method. Therefore, this article only discusses bilateral compensation. As shown in the figure 2.3, according to the different connection modes of the capacitors on both sides, common resonance compensation technologies can be divided into four structures: S-S, S-P, P-S, P-P (S denotes series and P denotes parallel). In addition, there are more complicated compensation networks such as CLC and LCC [20].

Since only S-S topology and CLC-S topology are used in the following text, we only analyze these two compensation topologies in detail here.

2.2.1 S-S compensation topology

When the inductors and the capacitors in the resonance state, we have,

$$\omega = \omega_0 = \frac{1}{\sqrt{LC}}, \quad (2.7)$$

where ω represents the working frequency, ω_0 represents the resonant angular frequency of the circuit. Here, to maximize the transmission efficiency of the WPT system, we need to make the resonant frequencies of the primary side and

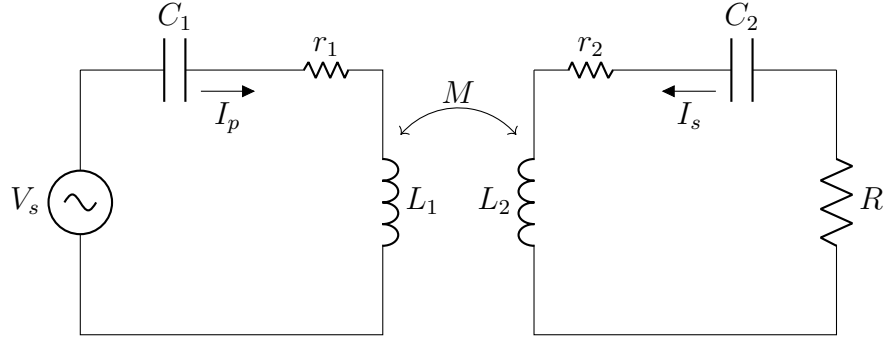


Figure 2.4: S-S structure.

secondary side consistent. Therefore,

$$\omega_0 = \frac{1}{L_1 C_1} = \frac{1}{L_2 C_2} \quad (2.8)$$

For any formed coil, we can measure its corresponding inductance value at a specified frequency. Thus, we can get the value of the compensation capacitor by formula 2.7.

$$C = \frac{1}{\omega_0^2 L} \quad (2.9)$$

$$V_R = \frac{j\omega M R}{(R + r_1)r_0 + \omega^2 M^2} V_s \quad (2.10)$$

2.2.2 CLC-S compensation topology

$$V_S = -jX_C I_S + jX_L I_L \quad (2.11)$$

$$V_0 = (-jX_{C_0} + jX_{L_0} + r_0)I_0 + j\omega M I_1 \quad (2.12)$$

$$V_R = j\omega I_0 + (-jX_{C_1} + jX_{L_1} + r_1)I_1 \quad (2.13)$$

$$V_R = -RI_1 \quad (2.14)$$

$$I_S = I_L + I_0 \quad (2.15)$$

$$V_R = -\frac{R}{R + r_1} \cdot \frac{\omega M}{X_L} V_S \quad (2.16)$$



Figure 2.5: CLC-S structure.

2.3 Underwater WPT system model

In the seawater environment, the electrical parameters of seawater as the transmission medium are quite different from those in the air, as shown in the table 2.1.

Table 2.1: The dielectric constant & conductivity of some materials at 25°C under 1kHz [21, 22].

Material	Relative permittivity	Conductivity
Vacuum	1	0 S/m
Air	1.0006	0 S/m
Ultra pure water	81	5.5×10^{-6} S/m
Drinking water	81	0.005 – 0.05 S/m
Seawater	81	5 S/m

It can be seen from table 2.1 that the relative permittivity of seawater is larger than that of air medium, resulting in a distributed capacitance between two conductors that are relatively close in seawater; at the same time, seawater has a certain conductivity , This is equivalent to connecting an eddy current loss resistor in series at both ends of the coil. Eddy current loss resistance and distributed capacitance will affect the impedance of the coil and generate additional power loss. Therefore, the conventional mutual inductance model of formula 2.5. cannot

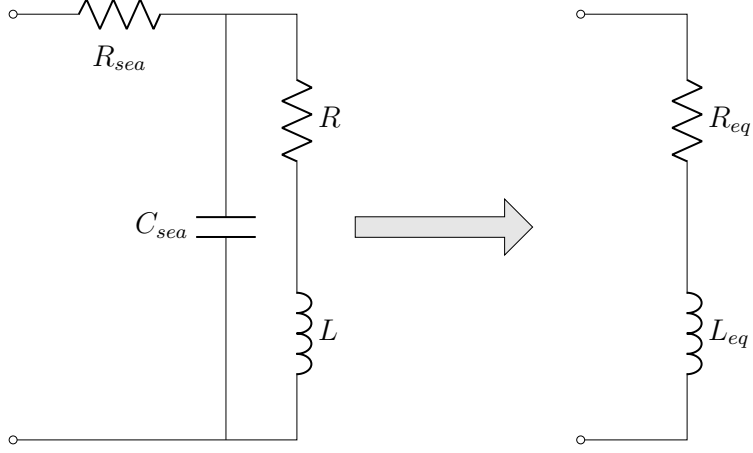


Figure 2.6: Equivalent circuit of the coil under seawater.

reflect the influence of seawater media on transmission, and cannot completely and accurately describe the transmission behavior under seawater.

As shown in figure 2.6, R_{sea} is the eddy current loss resistance, C_{sea} is the distributed capacitance, both of which increase with the increase of operating frequency, R is the internal resistance of the coil itself, and L is the coil inductance. The mathematical expressions of equivalent inductance L_{eq} and equivalent resistance R_{eq} are as follows,

$$L_{eq} = \frac{L - \omega^2 L^2 C_{sea} - C_{sea} R^2}{(1 - \omega^2 L C_{sea})^2 + \omega^2 C_{sea}^2 R^2}, \quad (2.17)$$

and

$$R_{eq} = R_{sea} + \frac{R}{(1 - \omega^2 L C_{sea})^2 + \omega^2 C_{sea}^2 R^2}. \quad (2.18)$$

Where ω is the operating angular frequency. Generally speaking, eddy current loss resistance R_{sea} and distributed capacitance C_{sea} are affected by many factors and are difficult to measure. Therefore, equations 2.17 and 2.18 are not easy to calculate, and they are usually obtained with three-dimensional electromagnetic field simulation software or experiments. Since R_{eq} is generally larger at high frequencies, underwater magnetic coupling resonance wireless energy transmission generally uses a working frequency below 1 MHz.

3 Preliminary exploration of underwater IPT system

In order to explore the similarities and differences between the wireless energy transmission system in the seawater environment and the wireless energy transmission system in the air in the actual situation, a simple double-coil structure is used to explore the electrical properties of the underwater environment. This chapter will introduce the performance of the double coil structure working in sea water.

3.1 The system in three different media

In order to design a wireless power transmission system suitable for underwater AUV, we will first use hollow cylindrical structure transmitter and cylindrical



(a) Experimental coil.



(b) Structure diagram.

Figure 3.1: Two-ring structure.

Table 3.1: The parameters of ring coil structure.

Items	Parameters
Environment	Air, tap water, seawater
Wire diameter	0.8mm
Wire material	Copper
Tx coil diameter	113mm
Rx coil diameter	85mm
Turns (Inner coil and outer coil)	10
Frequency	200kHz

structure receiver to explore the performance of the UWPT system of this plug-in structure UWPT in water. For the convenience of writing, it will be referred to as a double ring structure in the following text. The coil structure as shown in figure 3.1.

Its detailed parameters are shown in Table 3.1.

When we use the VNA analyzer to place the coil in the air, tap water, or seawater for measurement, the following data can be obtained:

$$Z_{air} = \begin{bmatrix} 0.4 + 29.6i & 0.0 - 10.0i \\ 0.0 - 10.0i & 0.3 + 20.3i \end{bmatrix},$$

$$Z_{tap-water} = \begin{bmatrix} 3.0 + 32.1i & -1.5 - 11.3i \\ -1.5 - 11.3i & 1.5 + 21.6i \end{bmatrix},$$

$$Z_{seawater} = \begin{bmatrix} 7.2 + 37.8i & -6.0 - 15.7i \\ -6.0 - 15.7i & 6.5 + 25.3i \end{bmatrix}.$$

In the above measurement results, we can find that as the transmission medium changes (from air to tap-water to seawater), each corresponding value is increasing. It illustrates that the internal resistances of the coils are small in the air. However, the internal resistances significantly increase when the coils are in tap-water or seawater. This may deteriorate the transmission efficiency as well as the load voltage stability. In addition, the mutual inductance between two coils becomes complex number and the self-inductances of the coils slightly increase.

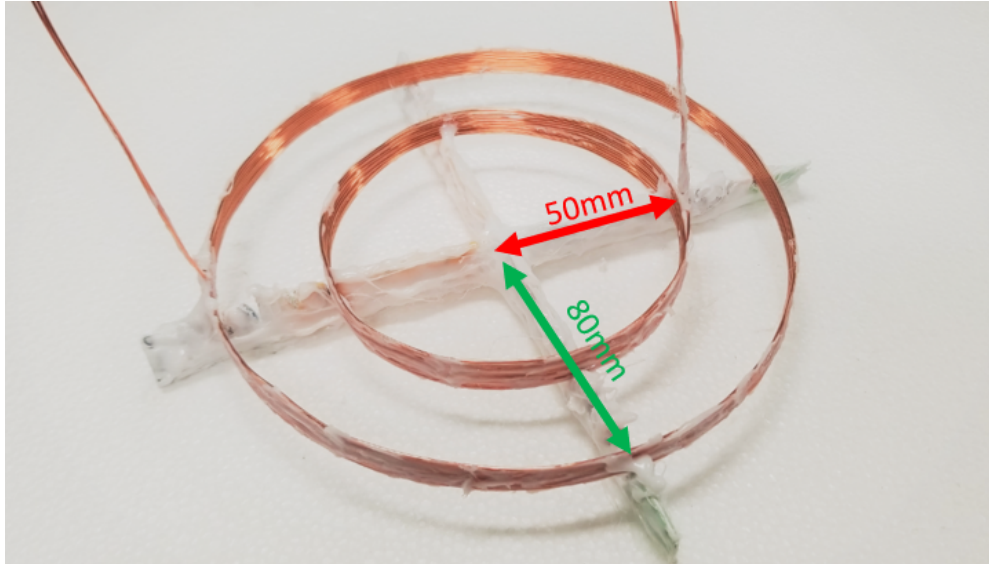


Figure 3.2: Two-ring structure ($r_{inner} = 50\text{mm}$, $r_{outer} = 80\text{mm}$).

3.2 The system in different sizes of the coil

In order to explore the influence of the size of the internal coil and the distance between the two coils on the system (Figure 3.2), the coil size is changed here to change the distance between the transmitter and the receiver. The specific parameters are as follows (Table 3.2).

After changing the medium between the coils and the distance between the coils, the Z-parameters in different scenarios are measured by VNA, and we get

Table 3.2: The parameters of ring coil structure.

Items	Parameters
Environment	Air, tap water, seawater
Wire diameter	0.8mm
Wire material	Copper
Tx coil diameter	160mm
Rx coil diameter	100mm, 120mm, 140mm
Turns (Inner coil and outer coil)	10
Frequency	200kHz

Table 3.3: Z-parameters in different distance and media

Media	Coil size (Radius)	Distance	Z-parameter
Air	80mm - 50mm	30mm	$\begin{bmatrix} 0.6826 + 46.4075i & -0.0411 - 8.9620i \\ -0.0382 - 8.9669i & 0.3423 + 24.2260i \end{bmatrix}$
	80mm - 60mm	20mm	$\begin{bmatrix} 0.7194 + 46.1416i & -0.0946 - 15.0048i \\ -0.0906 - 15.0155i & 0.5225 + 32.5246i \end{bmatrix}$
	80mm - 70mm	10mm	$\begin{bmatrix} 0.6657 + 45.9561i & 0.0757 + 24.2562i \\ 0.0699 + 24.2747i & 0.5651 + 39.2948i \end{bmatrix}$
Tap-water	80mm - 50mm	30mm	$\begin{bmatrix} 5.4603 + 53.0814i & -2.4332 - 11.7753i \\ -2.4304 - 11.7859i & 1.7722 + 26.0449i \end{bmatrix}$
	80mm - 60mm	20mm	$\begin{bmatrix} 7.0513 + 54.2993i & -4.4889 - 20.1926i \\ -4.4867 - 20.2100i & 3.9114 + 36.7652i \end{bmatrix}$
	80mm - 70mm	10mm	$\begin{bmatrix} 2.8768 + 49.8765i & 0.9991 + 26.5644i \\ 0.9946 + 26.5864i & 1.9865 + 42.0751i \end{bmatrix}$
Seawater	80mm - 50mm	30mm	$\begin{bmatrix} 1.761 + 58.2022i & -0.554 - 14.5303i \\ -0.5512 - 14.5424i & 0.6543 + 27.6708i \end{bmatrix}$
	80mm - 60mm	20mm	$\begin{bmatrix} 2.0488 + 61.1579i & -0.9906 - 25.1528i \\ -0.9814 - 25.1736i & 1.2212 + 40.4982i \end{bmatrix}$
	80mm - 70mm	10mm	$\begin{bmatrix} 2.0347 + 52.4298i & 0.4957 + 27.1092i \\ 0.4843 + 27.1321i & 1.4439 + 43.4828i \end{bmatrix}$

the following results (Table 3.3).

In table 3.3, we can find that under the same medium, as the internal coil decreases, the transmission distance increases. We can see that the imaginary part of Z_{11} and Z_{22} are increasing, indicating that the impedance of the coil is increasing.

Table 3.3 shows the measures of Z-parameter of the coupling network under

Table 3.4: The parameters of ring coil structure.

Items	Parameters
Environment	Air, seawater
Wire diameter	0.8mm
Wire material	Copper
Tx coil diameter	160mm
Rx coil diameter	100mm
Turns (Inner coil and outer coil)	10
Frequency	100kHz, 150kHz, 200kHz, 250kHz, 300kHz

several cases of coil sizes and distances in air, tap-water and seawater. In general, self-inductance of coil increases as coil size increases. The mutual inductance between two coils increases as the distance between them decreases. The internal resistances of the coils are small in air and larger in tapwater as well as seawater.

3.3 The system in different frequency

Earlier we have studied the z-parameter changes of the two-ring coil structure under different media and different distances. In this section we will study how z-parameters changes at different frequencies. Table 3.4 a shows the parameters of the experiment.

After using the above parameters, we got the following results (Table 3.5).

Table 3.5 shows that the internal resistances of the coils are less than 1Ω in the air when operating frequency changes from 100kHz to 300kHz. However, under seawater environment, the internal resistances of the coils are smaller than 1Ω when the operating frequency is under 200kHz. As the operating frequency is over 200kHz, the internal resistances of the coils significantly increase.

3.4 Conclusion

This section illustrated the measures of the coupling network in air, under tap-water and under seawater with different operating frequencies. The measures in-

Table 3.5: Z-parameters in different frequencies and media

Media	Frequency	Z-parameter
Air	100kHz	$\begin{bmatrix} 0.3758 + 23.2130i & -0.0036 - 4.4495i \\ -0.0012 - 4.4520i & 0.2123 + 12.1526i \end{bmatrix}$
	150kHz	$\begin{bmatrix} 0.4789 + 34.7320i & -0.0074 - 6.6739i \\ -0.0037 - 6.6774i & 0.2575 + 18.1971i \end{bmatrix}$
	200kHz	$\begin{bmatrix} 0.5755 + 46.2288i & -0.0121 - 8.9004i \\ -0.0050 - 8.9065i & 0.3031 + 24.2211i \end{bmatrix}$
	250kHz	$\begin{bmatrix} 0.6737 + 57.7432i & -0.0153 - 11.1342i \\ -0.0095 - 11.1426i & 0.3423 + 30.2465i \end{bmatrix}$
	300kHz	$\begin{bmatrix} 0.7556 + 69.2691i & -0.0191 - 13.3746i \\ -0.0100 - 13.3859i & 0.3791 + 36.2676i \end{bmatrix}$
Seawater	100kHz	$\begin{bmatrix} 0.5314 + 24.3255i & -0.0760 - 4.9832i \\ -0.0717 - 4.9862i & 0.2593 + 12.5247i \end{bmatrix}$
	150kHz	$\begin{bmatrix} 0.9900 + 39.2700i & -0.2453 - 8.8345i \\ -0.2392 - 8.8400i & 0.4080 + 19.6434i \end{bmatrix}$
	200kHz	$\begin{bmatrix} 2.0236 + 59.0193i & -0.7053 - 15.0451i \\ -0.6942 - 15.0581i & 0.7248 + 28.1895i \end{bmatrix}$
	250kHz	$\begin{bmatrix} 4.8486 + 89.4034i & -2.0763 - 26.6084i \\ -2.0597 - 26.6276i & 1.5345 + 39.8440i \end{bmatrix}$
	300kHz	$10^2 \times \begin{bmatrix} 0.1548 + 1.4909i & -0.0751 - 0.5327i \\ -0.0749 - 0.5333i & 0.0450 + 0.5985i \end{bmatrix}$

dicated that the internal resistances of the coils would increase when the system operated under tapwater or seawater. This would reduce transmission efficiency.

Moreoever, it could also make load voltage unstable against load variations even though CLC topology was employed. The internal resistances increased significantly as the operating frequency increased over 200kHz. Therefore, the system should operate at the frequency of lower than 200kHz under tapwater or seawater environment to restrict the loss caused by internal resistances.

4 Coil-array WPT

Through the explanation in the previous chapter, we know the basic performance of the wireless transmission system underwater. This chapter will introduce the underwater coil-array WPT system we designed, by degrading a large double coil structure into multiple small coil structures, as shown in figure 4.1. This greatly reduces the magnetic field in the internal coil, thereby achieving electromagnetic protection inside the AUV system. Its detailed parameters are shown in table 4.1.

In the marine environment, we can use buoys to generate electricity [1], store the collected electricity in the power source, and then connect the power source to the transmitter (Tx). When the AUV (Rx) reaches the designated position of the transmitter, the AUV can be charged wirelessly. This is the basic workflow of this UWPT system. Figure 4.2 shows a schematic diagram of the UWPT system.

In the following subsections, the performance of the coil-array UWPT system

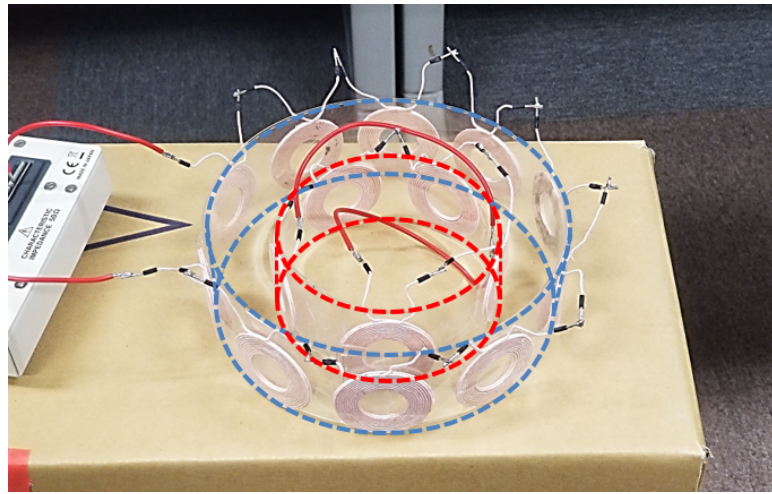


Figure 4.1: Coil-array structure.

Table 4.1: The parameters of coil-array structure.

Items	Parameters
Tx coil diameter	160mm
Rx coil diameter	100mm
The number of Tx coils	10
The number of Rx coils	5
Coil connection	In series
Coil model	WE 760308110 (Litz wire)

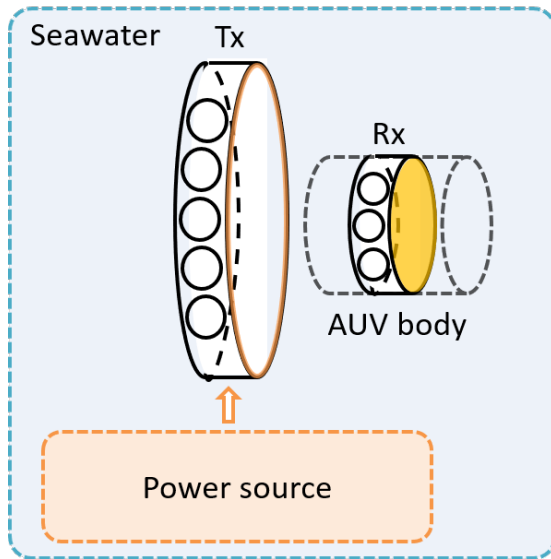


Figure 4.2: Sechematic diagram of coil-array UWPT system.

will be described in detail.

4.1 Measurement of the coil-array WPT system

In this section, we will first introduce different coil arrangements. By changing the coil structure of the coil-array, observe the performance of the changed coil structure under different conditions.

As shown in figure 4.3, a transmitter coil with a radius of 80mm is used here, which consists of 10 coils with ferrite in series, and a receiver coil with a radius



Parameters		Inner coil (Tx)	Outer coil (Rx)
Diameter		100mm	160mm
Number of coils		5	10
Material		Litz wire (2mm)	Litz wire (2mm)
200kHz	Q	207	206.25
	L	$125.01\mu H$	$241.03\mu H$
Position of inner coil		center	
L_s		$240.65\mu H$	
M		6.8923	
k		0.0397	
kQ		8.2007	
η_{max}		78.41%	

Figure 4.3: Coil-array IPT structure (Both sides with ferrite tile), inner coil in the center or the outer coil.

of 50mm, which consists of 5 coils with ferrite in series. Therefore, the distance between Tx and Rx is 30mm. For other specific parameters, please find in the figure 4.3.

By using LCR meter to measure this arrangement system, we can get the inductance of the Tx's coil-array coil, $L_1 = 241.03\mu H$, and quality factor $Q_1 = 206.25$. And the inductance of Rx's coil-array coil, $L_2 = 125.01\mu H$, and quality factor $Q_2 = 207$. Then short-circuit the Rx coil and place it in the middle of the Tx coil, and measure the inductance of the Tx in this state (As shown in figure 4.4), which is L_s , where $L_s = 240.65\mu H$.

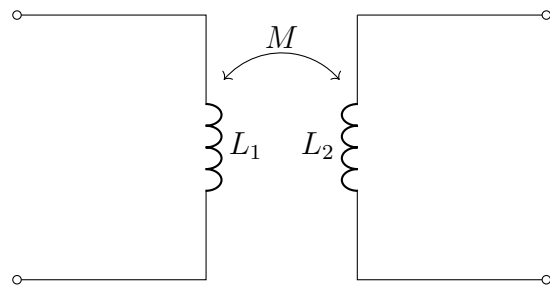


Figure 4.4: Measurement of L_s .

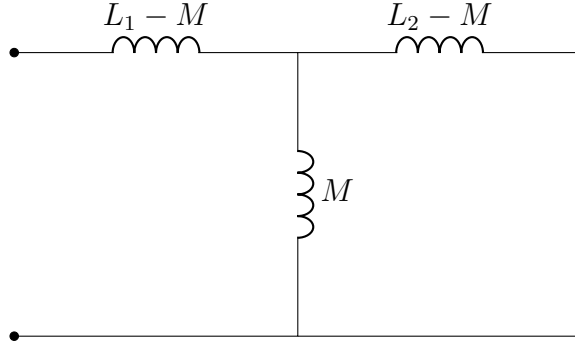


Figure 4.5: Equivalent circuit of two coil model.

From equivalent circuit (Figure 4.5), we can get the following formula.

$$L_s = L_1 - M + \frac{M(L_2 - M)}{L_2}. \quad (4.1)$$

Move M to the left side of the equation, the mutual inductance can be expressed as,

$$M = \sqrt{L_2(L_1 - L_s)}, \quad (4.2)$$

and coupling coefficient,

$$k = \frac{M}{L_1 L_2}. \quad (4.3)$$

kQ product can be expressed as,

$$kQ = k\sqrt{Q_1 Q_2}. \quad (4.4)$$

kQ product is an index showing the performance of a wireless transfer. The relationship between the maximum transmission efficiency η_{max} and kQ as follows [23, 24],

$$\eta_{max} = \frac{k^2 Q_1 Q_2}{(1 + \sqrt{1 + k^2 Q_1 Q_2})^2}. \quad (4.5)$$

According to the calculation of the above formula, we can get that the maximum transmission efficiency η_{max} of this arrangement is 78.41%.

4.2 The other coil arrangements and comparison

Next, we will observe the performance of the system under different conditions by increasing the number of coils and changing the position of the Rx coil in the Tx coil. The result is shown in the figure 4.6, figure 4.7, and figure 4.8.

Through the results under each of the above scenarios, we can summarize them into table 4.2, as follows

From table 4.2, we can get the following conclusions:

- When we increase the number of inner coils from 5 to 6, the maximum PTE (Power transfer efficiency) will increase.
- If the numbers of outer and inner coils are the same, when outer coils without ferrite and inner coils with ferrite, we can get the maximum PTE.
- When there is no ferrite outside the inner coil, the PTE will increase if the inner coil deviates from the middle, and vice versa.

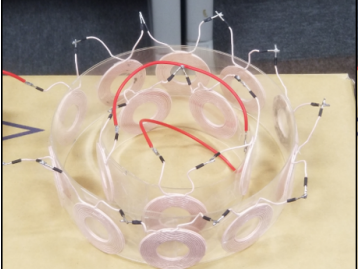
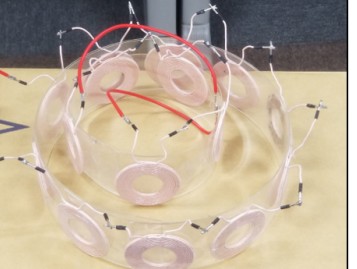
Number of outer coils		Number of inner coils	
10	5		
			
M	4.2371	M	8.9941
k	0.0428	k	0.0909
kQ	7.5365	kQ	15.9979
η_{max}	76.75%	η_{max}	88.26%

Figure 4.6: Coil-array IPT structure (both sides without ferrite tile), inner coil in the center of the outer coil (left), inner coil next to the outer coil (right).

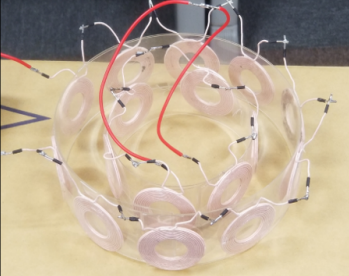
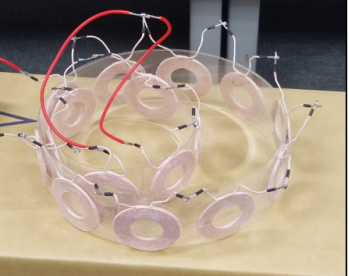
Number of outer coils		Number of inner coils	
10	6		
			
M	4.7709	M	13.4385
k	0.0446	k	0.1255
kQ	7.6436	kQ	21.5303
η_{max}	77.03%	η_{max}	91.13%

Figure 4.7: Coil-array IPT structure (both sides without ferrite tile), inner coil in the center of the outer coil (left), inner coil next to the outer coil (right).

Table 4.2: Maximum power transfer efficiency of different coil arrangements.

Shift	Numbers of coil (Outer - Inner)	Both coils with ferrite	Both coils without ferrite	Outer coils without ferrite, inner coils with ferrite
Inner coil in the center	10 - 5	78.41%	76.75%	84.95%
	10 - 6		77.03%	
Inner coil close to the one side	10 - 5		88.26%	78.80%
	10 - 6		91.13%	

4.3 Magnetic field distribution

In order to clarify the magnetic field distribution of the coil-array structure, we used Wipl-d electromagnetic simulation software. We simulated the following two

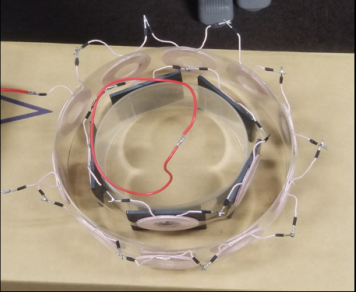
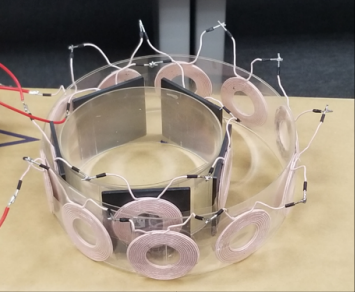
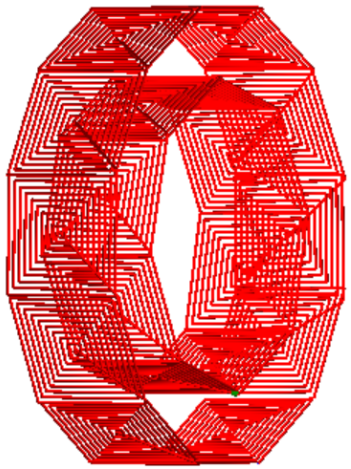
Number of outer coils		Number of inner coils	
10	5		
			
M	8.3363	M	5.8093
k	0.0629	k	0.0435
kQ	12.2445	kQ	8.3768
η_{max}	84.95%	η_{max}	78.81%

Figure 4.8: Coil-array IPT structure (inner small coils with ferrite tile, outer small coils without ferrite tile), inner coil in the center of the outer coil (left), inner coil next to the outer coil (right).

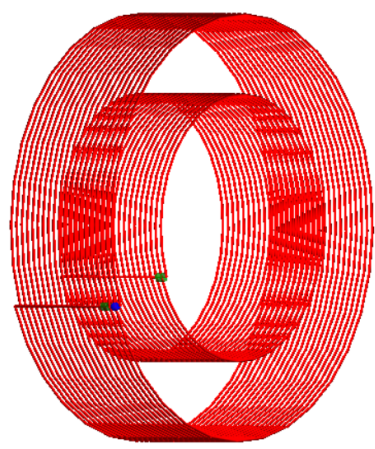
Table 4.3: The parameters of two coil structure in simulation.

Items	Coil-array structure	Two-ring structure
Tx coil diameter	160mm	160mm
Rx coil diameter	100mm	100mm
The number of Tx coils	12	1
The number of Rx coils	8	1
Wire material	Copper	Copper
Frequency	200kHz	200kHz
Resistance of load	5Ω	5Ω
Voltage of source	6v	64v
Output power	10w	10w

structures as shown in figure 4.9, and the specific parameters are as table 4.3.



(a) Coil-array IPT structure.



(b) Two-ring IPT structure.

Figure 4.9: Two kind of UWPT coil structure simulation diagram.

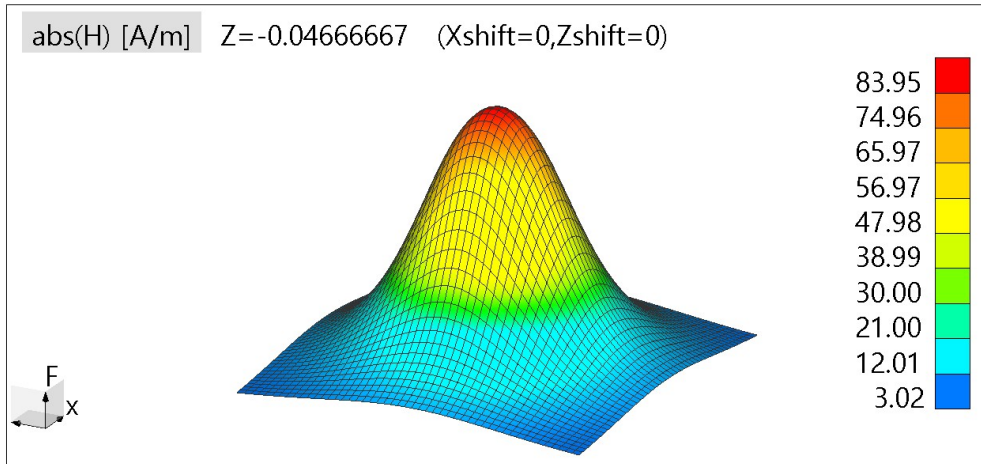


Figure 4.10: Magnetic field distribution of two-ring IPT structure.

4.3.1 Magnetic field distribution of two-ring strcuture

In order to judge whether the coil-array structure can reduce the internal magnetic field strength of the AUV system, we first simulated the traditional two-ring system. The results are shown in figure 4.10 and figure 4.11. figure 4.10 shows the magnetic field distribution between the transmitting and receiving coils in a three-dimensional space. The highest peak in the figure is the middle of the two

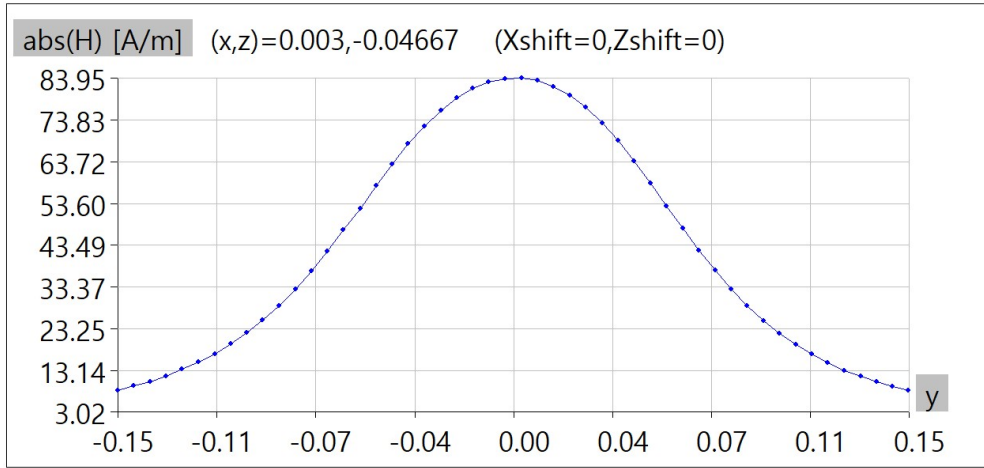


Figure 4.11: Cross-sectional view of the magnetic field distribution of two-ring IPT structure.

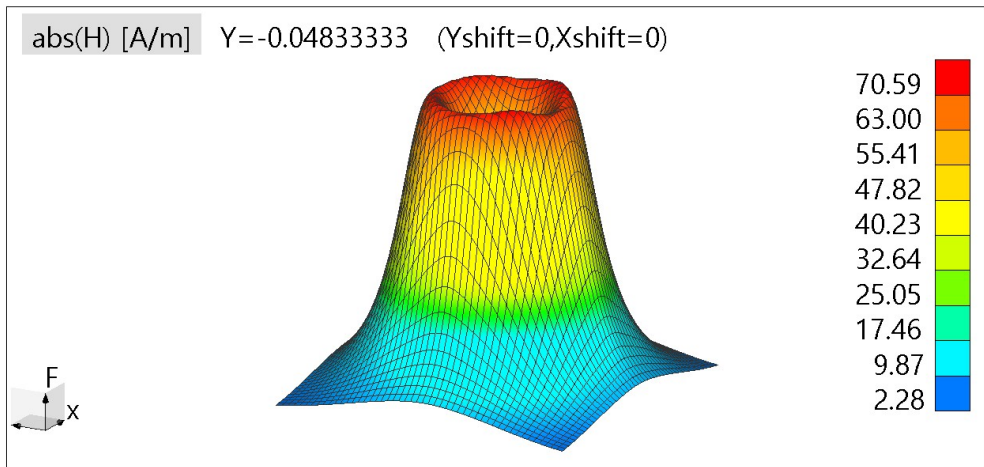


Figure 4.12: Magnetic field distribution of coil-array IPT structure.

coils, that is, the magnetic field distribution shown in figure 4.10 is generated inside the AUV. figure 4.11 is a cross-sectional view of figure 4.10 from the side. We can see that the magnetic induction intensity of the middle part has reached $83.95\text{A}/\text{m}$, and the other parts are gradually decreasing, like a mountain.

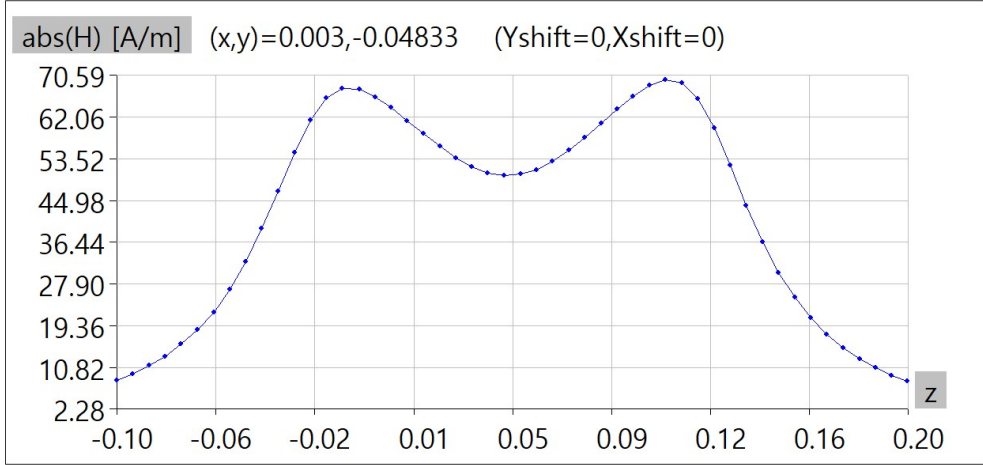


Figure 4.13: Cross-sectional view of the magnetic field distribution of a coil-array IPT structure.

4.3.2 Magnetic field distribution of coil-array structure

After completing the simulation of the magnetic field distribution of the two-ring structure, we did the same simulation on the coil-array structure coil, and the results are shown in figure 4.12 and figure 4.13. In figure 4.12, we can see that the magnetic field distribution of the coil-array structure is like a volcano, with low magnetic induction in the middle part and high surrounding magnetic induction. The part with the highest magnetic induction is between the two coils, that is, outside the AUV, which will not affect the inside of the AUV system. From figure 4.13 we can see that the internal magnetic field of the AUV is around 50A/m, which is 40% lower than the two-ring structure, and its large magnetic induction intensity is lower than 70A/m, which is lower than the highest magnetic induction intensity of the two-ring structure 13A/m.

4.4 PET over shift in two directions

Since both the coil-array and the two-ring are hollow cylindrical structures transmitter, the rotation of the receiver coil will not have much impact on the system transmission efficiency. This section will explore the offset effect of these two structures in the horizontal direction and vertical direction. Suppose the hori-

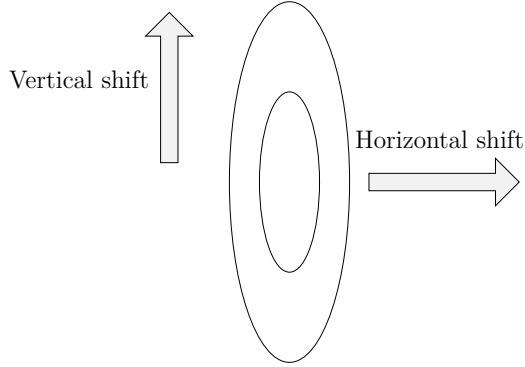


Figure 4.14: Equivalent circuit of two coil model.

zontal offset and vertical offset are specified as shown in figure 4.14.

We first offset the internal coils of the two structures from 0 to 100mm in the horizontal direction to obtain the result in Figure 1. The red line part is the coil-array structure, and the blue part is the two-ring structure. From the figure, we can find that when Rx is in the center of Tx, the transmission efficiency of the two-ring structure is 95%, while the transmission efficiency of the coil-array structure is 60%. And when the horizontal offset increases, the transmission efficiency of the coil-array structure changes greatly, and when the offset is 100mm, the PTE is close to 0. The PTE of the two-ring structure remains basically unchanged.

This is because the coupling of the coil-array structure is completed by small coils. When the horizontal offset exceeds the size of the coil, the opposite circular coil cannot be coupled well, so the PET drops sharply. The coupling of the two-ring structure is the coupling between two hollow cylindrical coils, like two solenoid, so even when a large displacement occurs in the horizontal direction, the PTE can basically remain unchanged.

Figure 4.15 (b) shows the offset in the vertical direction. We can see that the red line representing the coil-array structure increases with the horizontal offset of the Rx coil, that is, the Tx coil and the Rx coil are getting closer, and the PTE of the system is also constantly increase. When the offset reaches 25mm, the PTE of the system is close to 90%.

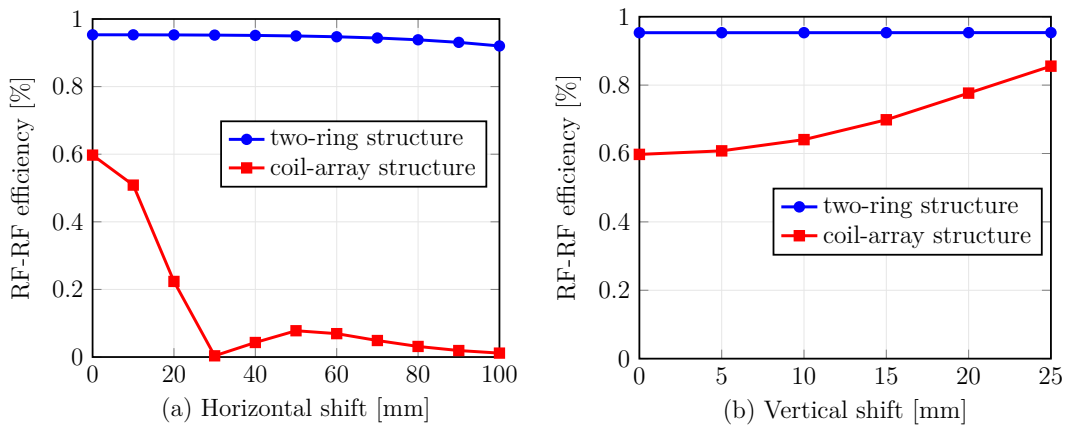


Figure 4.15: The PET over shift in two different directions.

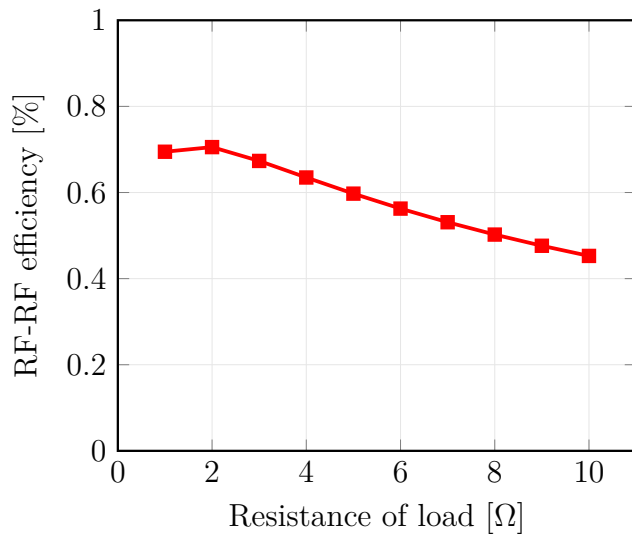


Figure 4.16: The PET over different resistance of load (coil-array structure).

5 Conclusion

5.1 Future works

Acknowledgements

First of all, I would like to thank my supervisor, Professor Minoru Okada. Professor Okada is kind, knowledgeable, and rigorous in scientific attitude. Thank him for giving me an opportunity to study in Japan and let me do wireless power transfer research that I am interested in. He has continued to help me during my three years of study and life. At the same time, I would like to thank Professor Yuichi Hayashi for my research advice and guidance, so that I have a deeper understanding of the weak research environment. With his help, Which greatly improved my research.

Then I would like to thank Associate Professor Takeshi Higashino and Assistant Professor Duong Quang Thang. With their help, they have made me better understand the knowledge of wireless power transfer and wireless communication, and they have helped me overcome the difficulties in professional understanding and helped me complete this topic. Thank them very much. Here, I would also like to thank Assistant Professor Chen Na for her continuous help and encouragement in my studies, so that I have a better understanding of the field of communication.

I would also like to thank the members, staff, and seniors of the Network Systems Laboratory for their companionship in the study and life. We studied together and played together, and established a strong friendship together. Thank you to the international students who have helped me while studying abroad. Thank you for your kindness to me.

Finally, I would like to thank my family for their support of studying abroad, let me choose the knowledge I like, and always provide me with abundant financial support.

Thank you all for your kind help again.

References

- [1] P. Z. Taofeek Orekan, *Underwater Wireless Power Transfer*. Springer-Verlag GmbH, Dec. 2018. [Online]. Available: https://www.ebook.de/de/product/35055522/taofeek_orekan_peng_zhang_underwater_wireless_power_transfer.html
- [2] J. Randhawa, “Ocean energy: The future of renewable energy,” 07 2015.
- [3] J. Heidemann, M. Stojanovic, and M. Zorzi, “Underwater sensor networks: applications, advances and challenges,” *Philosophical Transactions of the Royal Society A: Mathematical, Physical and Engineering Sciences*, vol. 370, no. 1958, pp. 158–175, jan 2012.
- [4] W. Wu, Z. Zhang, W. Lee, and D.-Z. Du, “Underwater sensors,” in *Optimal Coverage in Wireless Sensor Networks*. Springer International Publishing, 2020, pp. 257–260.
- [5] J. Hwang, N. Bose, and S. Fan, “AUV adaptive sampling methods: A review,” *Applied Sciences*, vol. 9, no. 15, p. 3145, aug 2019.
- [6] N.-H. Tran, T.-D. Huynh, T.-P. Ton, and T.-H. Huynh, “Design of depth control for hybrid AUV,” in *Lecture Notes in Electrical Engineering*. Springer International Publishing, aug 2020, pp. 521–531.
- [7] A. Bradley, M. Feezor, H. Singh, and F. Y. Sorrell, “Power systems for autonomous underwater vehicles,” *IEEE Journal of Oceanic Engineering*, vol. 26, no. 4, pp. 526–538, 2001.
- [8] R. Jurdak, C. Lopes, and P. Baldi, “Battery lifetime estimation and optimization for underwater sensor networks,” *IEEE Sensor Network Operations*, 05 2006.

- [9] V. E. B. Anand Nayyar, *International Conference on Innovative Computing and Communications*. Springer-Verlag GmbH, Nov. 2018. [Online]. Available: https://www.ebook.de/de/product/34849820/international_conference_on_innovative_computing_and_communications.html
- [10] T. Wang, D. Li, C. Yang, M. Lin, and T. Zhang, “Non-contact wet mate connectors for subsea observation networks,” in *OCEANS 2016 MTS/IEEE Monterey*. IEEE, sep 2016.
- [11] S. C. Capareda, “Tidal energy,” in *Introduction to Renewable Energy Conversions*. CRC Press, aug 2019, pp. 239–264.
- [12] B. Drew, A. R. Plummer, and M. N. Sahinkaya, “A review of wave energy converter technology,” *Proceedings of the Institution of Mechanical Engineers, Part A: Journal of Power and Energy*, vol. 223, no. 8, pp. 887–902, dec 2009.
- [13] J. G. Vlachogiannis, “Marine-current power generation model for smart grids,” *Journal of Power Sources*, vol. 249, pp. 172–174, mar 2014.
- [14] Q. Zeng, J. Ma, J. Mo, and Y. Zhang, “Extracting salt difference energy with silicon nitride nanopore generator,” in *2020 5th International Conference on Power and Renewable Energy (ICPRE)*. IEEE, sep 2020.
- [15] Wikipedia contributors, “Wireless power transfer — Wikipedia, the free encyclopedia,” 2021, [Online; accessed 23-January-2021]. [Online]. Available: https://en.wikipedia.org/w/index.php?title=Wireless_power_transfer&oldid=1001183613
- [16] C. M. Chun T. Rim, *Wireless Power Transfer for Electric Vehicles and Mobile Devices*. IEEE COMPUTER SOC PR, Aug. 2017. [Online]. Available: https://www.ebook.de/de/product/29045715/chun_t_rim_chris_mi_wireless_power_transfer_for_electric_vehicles_and_mobile_devices.html
- [17] Z. Zhang, H. Pang, A. Georgiadis, and C. Cecati, “Wireless power transfer—an overview,” *IEEE Transactions on Industrial Electronics*, vol. 66, no. 2, pp. 1044–1058, feb 2019.

- [18] B. Song, Y. Wang, K. Zhang, and Z. Mao, “Research on wireless power transfer system for torpedo autonomous underwater vehicles,” *Advances in Mechanical Engineering*, vol. 10, no. 9, p. 1687814018802563, 2018. [Online]. Available: <https://doi.org/10.1177/1687814018802563>
- [19] Y. Wang, B. Song, and Z. Mao, “Application of shielding coils in underwater wireless power transfer systems,” *Journal of Marine Science and Engineering*, vol. 7, no. 8, 2019. [Online]. Available: <https://www.mdpi.com/2077-1312/7/8/267>
- [20] C. Jiang, K. T. Chau, C. Liu, and C. H. T. Lee, “An overview of resonant circuits for wireless power transfer,” *Energies*, vol. 10, no. 7, p. 894, jun 2017.
- [21] Wikipedia contributors, “Relative permittivity — Wikipedia, the free encyclopedia,” 2020, [Online; accessed 23-January-2021]. [Online]. Available: https://en.wikipedia.org/w/index.php?title=Relative_permittivity&oldid=991278612
- [22] Lenntech, “Water conductivity - lenntech,” 2021. [Online]. Available: <https://www.lenntech.com/applications/ultrapure/conductivity/water-conductivity.htm>
- [23] S. Li and C. C. Mi, “Wireless power transfer for electric vehicle applications,” *IEEE Journal of Emerging and Selected Topics in Power Electronics*, vol. 3, no. 1, pp. 4–17, mar 2015.
- [24] T. Ohira, “Extended k-q product formulas for capacitive- and inductive-coupling wireless power transfer schemes,” *IEICE Electronics Express*, vol. 11, no. 9, pp. 20 140 147–20 140 147, 2014.